Journal of Materials Chemistry A

PAPER

View Article Online
View Journal | View Issue

Cite this: J. Mater. Chem. A, 2017, 5, 20422

Monolithic laser scribed graphene scaffolds with atomic layer deposited platinum for the hydrogen evolution reaction†

Pranati Nayak,‡[ab] Qiu Jiang,‡[a] Narendra Kurra,‡[a] Xianbin Wang,[a] Ulrich Buttner[a] and Husam N. Alshareef *[a]

Received 17th July 2017
Accepted 31st August 2017

DOI: 10.1039/c7ta06236b

rsc.li/materials-a

Three-dimensional (3D) electrode architectures for conformal deposition and effective use of catalysts are an emerging area with significant interest in electrocatalytic applications. In this study, we report the fabrication of monolithic, self-standing, 3D graphitic carbon scaffolds with conformally deposited Pt by atomic layer deposition (ALD) as a hydrogen evolution reaction catalyst. Laser scribing is employed to transform polyimide into 3D porous graphitic carbon, which possesses good electronic conductivity and numerous edge plane sites. This laser scribed graphene (LSG) architecture makes it possible to fabricate a monolithic electrocatalyst support without any binders or conductive additives. The synergistic effect between the ALD of Pt and the 3D network of LSG provides an avenue for minimal yet effective usage of Pt leading to an enhanced HER activity. This strategy establishes a general approach for inexpensive and large scale HER device fabrication with minimum catalyst cost.

Introduction

The limited availability of traditional fossil fuels and the adverse environmental health issues resulting from their massive consumption demand for developing alternate clean and renewable energy sources essential.[1,2] Hydrogen is considered as the cleanest carbon-free molecular fuel and green energy carrier for various applications.[3,4] However, currently the commercial production of hydrogen primarily relies on the steam methane reforming route, which is being sourced mainly from fossil reserves. This technology seems to be unviable since it involves a high energy (heat) input followed by a substantial amount of CO_2 release as a by-product.[5,6] Interestingly, water splitting is an eco-friendly methodology for H_2 production, which can be realized *via* electrochemical, photochemical, and photoelectrochemical techniques. A significant amount of research has been directed towards electrochemical water splitting which is potentially green and renewable for hydrogen production without CO_2 emissions.[7] However, for efficient H_2 production, the optimal design of electrocatalysts is required to speed up the hydrogen evolution reaction (HER) kinetics.[8] To date, various noble metals and semiconductors have been used as catalysts for the HER. Apparently, metallic platinum (Pt) remains as an unbeatable catalyst due to its unprecedented catalytic activity in liberating H_2 from a pair of protons and electrons at high reaction rates and low overpotentials (η).[9,10] For scaled up applications, the prohibitive cost of Pt remains as the biggest obstacle to its use.

Researchers have identified two main strategies to cope with the expensive cost of Pt by replacing or reducing Pt consumption to achieve sustainable H_2 production. Electrocatalysts based on transition metals such as Fe, Co, Ni, and Mo and their molecular derivatives have been employed as alternatives to expensive Pt.[11,12] However, the cycling stability of these catalysts was found to be mediocre as they are prone to corrosion by acid electrolyte. Transition metal dichalcogenides and carbides such as MoS_2 and Mo_2C have also shown excellent electrocatalytic activity towards the HER. However, their poor electronic conductivity prevents their use for commercial device fabrication.[13] In this scenario, developing a technology that will markedly minimize the Pt use and in parallel increase its utilization efficiency is a key step for the future 'hydrogen economy'. One strategy could be employing Pt at the atomic scale supported on high surface area conducting carbon architectures for its minimum and effective utilization. Design schemes like anchoring Pt on 1D carbon nanotubes (CNTs), 2D graphene, g-C_3N_4, porous carbon, hetero-atom doped graphene have been reported to improve the HER activity and long-term stability with minimal Pt usage.[14–16] However, these highly efficient electrocatalysts used under an experimental framework have the form of fine powder. Hence, polymeric binders,

[a]Materials Science and Engineering, Physical Sciences & Engineering Division, King Abdullah University of Science and Technology (KAUST), Thuwal, 23955-6900, Saudi Arabia. E-mail: husam.alshareef@kaust.edu.sa

[b]Electrodics and Electrocatalysis (EEC) Biosensor Division, CSIR-Central Electrochemical Research Institute (CSIR-CECRI), Karaikudi, Tamilnadu, 630006, India

† Electronic supplementary information (ESI) available. See DOI: 10.1039/c7ta06236b

‡ These authors contributed equally to the work.

surfactants and extra conductive additives are needed during slurry preparation to make the film intact and conductive.[17–21] These additives result in devices with poorly controlled structures, plenty of dead volumes, and adverse sites that are unfavorable for electron conduction. Additionally, the use of solution processing (slurry making) restacks the materials, which limits the electrochemically active surface area and blocks the active sites of electrocatalysts resulting in an increase in resistance to mass transfer.[22] Also, mass production of identical devices with high reproducibility in performance is still an issue. Therefore, fabricating a 3D self-standing, flexible, porous and conductive monolithic support is highly desirable for incorporating electrocatalysts into 3D scaffolds, which resolves the above stated issues associated with the device fabrication of powder electrocatalysts. These 3D conductive networks provide high specific surface area, which facilitates the ion diffusion, catalyst–electrolyte interaction and finally the electron transport during electrocatalytic processes, thus improving the reaction kinetics and overall HER performance.

Atomic layer deposition (ALD) is a powerful tool for precisely controlled dispersion of catalysts on a substrate, which prevents their agglomeration and promotes their effective utilization. ALD is capable of controlling the thickness of Pt to the monolayer scale, resulting in excellent HER activity.[23] Recently, Saha *et al.* demonstrated the HER activity of Pt coated Mo_2C by ALD.[24] Katuri *et al.* have employed Pt coating over 3D polymeric hollow fiber membranes by ALD for the recovery of both H_2 energy (through the HER) and fresh water concurrently followed by waste-water treatment.[25]

In this study, we employ a direct-write laser technique to fabricate a binder-free, monolithic, porous, conductive 3D interconnected network of 2D graphene sheets (henceforth referred to as laser scribed graphene or LSG) from commercial polyimide (PI). The self-standing scaffold is rich in edge plane sites but still functional enough to be wetted by aqueous electrolytes. These flexible LSG electrodes were then conformally coated with Pt using ALD (Pt/LSG). The loading of the Pt catalyst is precisely controlled by tuning the number of ALD cycles and we did a systematic study on its HER activity. The Pt/LSG electrodes show promise for the best utilization of the catalyst with much less Pt loading signified by the high current density comparable to that of a commercial Pt catalyst. Also a very good stability with high reproducibility is observed for Pt/LSG electrodes.

Results and discussion

Fig. 1a shows a schematic illustrating the fabrication of LSG electrodes on a PI sheet using a laser scribing technique. It has been previously demonstrated that the energetic laser beam could transform insulating PI into conductive graphitic carbon that was employed as an electrode for supercapacitors and electrochemical sensors.[26,27] The *X*–*Y* translational movement of the laser beam would allow scalable fabrication of graphitic carbon electrodes on a PI sheet in a desirable fashion. The intrinsic chemical inertness of the LSG scaffold may not be a good choice of electrocatalyst by itself. However, sensitization

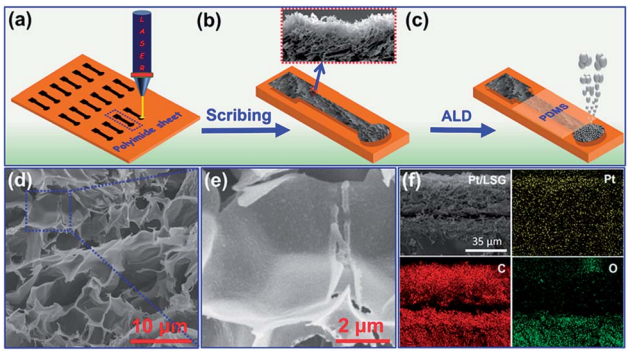

Fig. 1 Schematic illustration of the fabrication of LSG and Pt/LSG electrode patterns on a PI sheet: (a) fabrication of arrays of electrodes on the PI sheet by laser scribing, (b) 3D view of the LSG electrode pattern. The projection displays a vertical cross-sectional SEM image of a laser scribed PI sheet showing the highly porous and protruded morphology of graphene, (c) selective passivation of the electrode area by using PDMS and ALD of Pt selectively on the working electrode area, (d and e) SEM and high resolution SEM images of homogeneously coated ALD Pt over laser scribed graphene, (f) the cross-sectional SEM micrograph and its corresponding elemental mapping images for C K, O K and Pt M.

with a metal catalyst could be a potential option, especially using a conformal deposition process that can effectively cover the 3D porous architecture of LSG (Fig. 1b and c). The morphology of the as-obtained LSG and Pt/LSG using different numbers of ALD cycles was characterized using SEM. The morphology of LSG is seen to be porous from a 3D perspective, abundant of edge-plane sites as shown in the SEM micrographs (see Fig. 1b projection and ESI, Fig. S1†). In fact, the focused laser beam helps in carbonization and graphitization of PI surfaces due to very high local temperatures (>2500 °C).[26] Concurrently, the local availability of oxygen and moisture in air during the graphitization process could burn-off some amount of carbon in the form of gaseous CO and CO_2, which makes LSG porous with less oxygen content. The intact 3D morphology offers high accessible electrochemical surface area, whereas the edge-plane rich morphology of LSG patterns is anticipated to enhance catalytic activity.[27,28] Furthermore, the catalytic activity of LSG was enhanced through surface coating of Pt by atomic layer deposition (ALD) (scheme shown in Fig. 1c). ALD is a unique technique because of its ability for conformal deposition of materials onto 3D architectures.[25] As LSG is highly porous, Pt deposition by ALD could ensure the uniform and homogeneous coverage of an ultra-thin Pt layer. Fig. 1d–e illustrate the top-view SEM and high resolution SEM images of the Pt/LSG. The homogeneous deposition of Pt on LSG by ALD is confirmed by the SEM elemental mapping (shown in Fig. 1f and S2a–c†). The EDX spectrum shown in Fig. S2g† confirms the presence of Pt in the Pt/LSG sample. The loading of Pt on Pt/LSG electrodes was measured by calculating the weight difference after and before ALD cycles (shown in Fig. S2h†). The relatively small mass loading (0.04 mg cm^{-2} for 200 cycle ALD) of platinum on LSG compared to a commercial Pt/C catalyst (0.5 mg cm^{-2}), which is nearly an order of magnitude lower mass loading compared to commercial Pt/C indicates the minimal yet effective usage of Pt by this ALD technique.

XRD and Raman spectroscopy were employed to investigate the structural characteristics of Pt/LSG electrodes. The XRD pattern (Fig. S3†) of the as-prepared LSG confirms the graphitic structure as evidenced by the presence of the typical C (002) peak at $2\theta = 26.42^\circ$ with a corresponding interlayer spacing of $\approx$0.34 nm (d_{002}). The broad nature of the C (002) peak depicts disorder in the c-axis periodicity of the 3D graphitic structure.[29] However, well-resolved peaks were obtained at $2\theta = 35^\circ$ and 70° for Pt/LSG (Fig. 2a), which can be indexed to the simple cubic structure of Pt (JCPDS no-87-0646).[30] The nature of graphitic carbon produced using a laser scribing process was analyzed using Raman spectroscopy. Raman spectroscopy is a good structural characterization tool for carbon materials, especially graphitic type materials as their π-electrons can be polarized easily giving higher scattering cross sections.[31] As shown in Fig. 2b, three dominant peaks are observed: the D band (induced by bent sp^2 carbon bonds by breaking translational symmetry, essentially defect sites/functional groups), G band (corresponds to the E_{2g} vibration mode of graphitic carbon), and 2D band which is due to the periodicity and alignment of graphene layers along the *c*-axis.[31,32] Similar Raman signatures were observed at different regions of the LSG sample. The typical D band position is observed at 1365.8 cm^{-1} with a FWHM of 53.7 cm^{-1}, the G band at 1583.5 cm^{-1} with a FWHM of 36.3 cm^{-1} and the 2D band at 2724.2 cm^{-1} with a FWHM of 76.2 cm^{-1}. Though the 2D band is seen as a single symmetric peak, its broadness up to 76 cm^{-1} is a clear indication of the turbostratic nature of graphene sheets in LSG.[33] The laser scribing process seems to trigger the depolymerization of PI, causing subsequent carbonization and graphitization, resulting in the formation of the graphitic domains. As this process is carried out under ambient conditions, the available surplus oxygen and water molecules in the surrounding environment under such high temperature conditions react with graphitic carbon releasing some of it in the form of CO and CO_2 gases. However, the non-uniform distribution of oxygen, water molecules and intense laser energy produces an intricate morphology of 3D porous graphitic carbon in this laser scribing process. The details of Raman spectral features are tabulated in Table S1 in the ESI.† The typical I_D/I_G ratio for Pt/LSG is found to be in the range of 0.2–0.23, and corresponding graphitic crystallite size is ~50 nm, estimated using the following equation.[34]

$$L_a\ (\text{nm}) = 560/E_{\text{laser}}{}^4(I_D/I_G)^{-1} \quad (1)$$

where E_{laser} is the laser excitation energy in eV.

As shown in Fig. 2c, the I_D/I_G map shows an average value of 0.21 (well in agreement with previous reports) and uniform distribution of defects, which could be beneficial for providing more electrochemically active sites and improving the catalytic activity.[26] Further, the elemental composition and chemical state of individual elements were studied by X-ray photoelectron spectroscopy. Fig. S4 shows the XPS analysis and the details are discussed in ESI.†

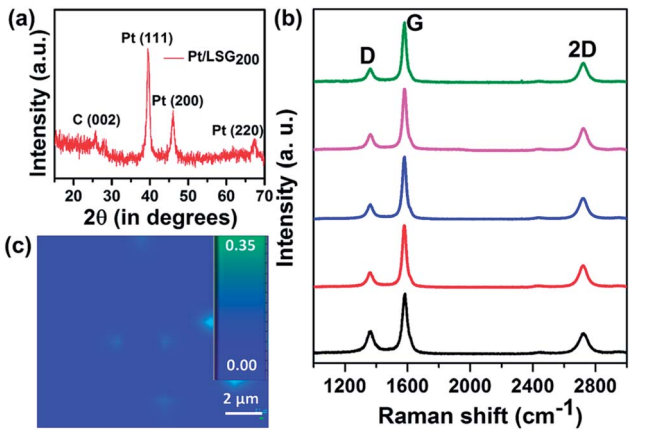

Fig. 2 (a) XRD pattern of the Pt/LSG electrodes, (b) Raman spectra at different regions on Pt/LSG showing the uniform nature of graphitic carbon produced from the laser scribing process, and (c) I_D/I_G map of Pt/LSG over a 10 × 10 μm area showing the uniform distribution of defects, indicating numerous available edge planes.

Electrochemical activity and durability

The electrocatalytic HER performance of the as-prepared LSG and Pt/LSG electrodes were compared by conducting linear sweep voltammetry (LSV) at 5 mV s^{-1} in 0.5 M H_2SO_4 utilizing a conventional three-electrode set up consisting LSG as the working electrode, Pt wire as the counter electrode, and Ag/AgCl (3 M KCl) as the reference electrode (Fig. 3a). To make a comparison, a commercial Pt/C catalyst cathode (10 wt% on Vulcan XC-72R carbon black) was also tested under the same conditions. The commercial Pt/C catalysts were mixed with Nafion solution followed by drop-casting on a glassy carbon electrode for HER tests (details discussed in the ESI†). The

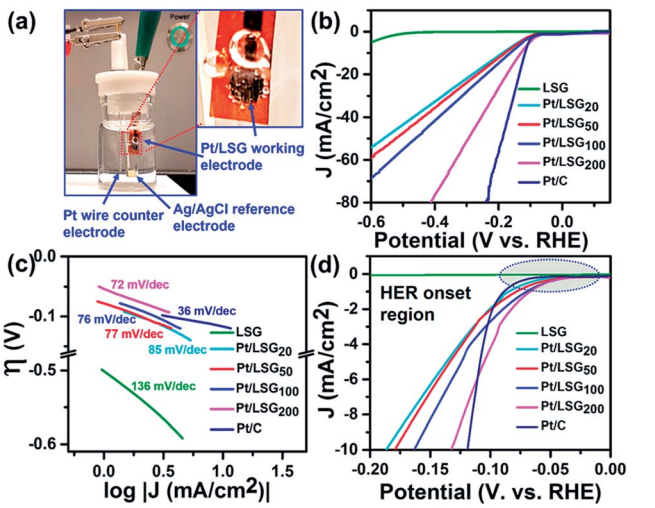

Fig. 3 Electrochemical performance of Pt/LSG electrodes compared to bare LSG and commercial Pt/C in 0.5 M H_2SO_4 electrolyte. (a) Digital photograph showing a 3 electrode system comprising a LSG based electrode as the working electrode, Pt wire as the counter electrode and Ag/AgCl as the reference electrode. The photograph was taken when the cell was turned on for 20 s. Inset showing H_2 bubble formation upon the start of the LSV cycle, (b) LSV and (c) Tafel plots of Pt/LSG electrodes at a varied number of ALD cycles compared to LSG and commercial Pt/C, (d) LSV showing the HER onset region for LSG and Pt/LSG electrodes compared to commercial Pt/C.

electrochemical polarization curves of LSG and Pt/LSG based electrodes are plotted in Fig. 3b. The HER onset overpotential of the as-prepared LSG electrode was determined to be ≈0.667 V, indicating little activity towards hydrogen evolution. However, Pt/LSG_{20} showed a substantial decrease of the onset potential to 0.188 V. Furthermore, as the Pt content was increased by the number of ALD cycles, the onset potential of Pt/LSG electrodes gradually decreased. The specific activity of all samples was calculated from the polarization curves by normalizing the current with the geometric area of the electrodes. Further investigation of the HER activity was done by fitting the linear region of the Tafel plot using the Tafel equation.[24]

$$\eta = a + b\log|J| \quad (2)$$

where, η is the overpotential, J is the current density, b is the Tafel slope and 'a' is the intercept of the plot. The Tafel plots of each LSG and Pt/LSG electrode were compared as shown in Fig. 3c. The Tafel slopes of Pt/C, LSG, Pt/LSG_{20}, Pt/LSG_{50}, Pt/LSG_{100} and Pt/LSG_{200} were found to be ≈36, 136, 85, 77, 76, and 72 mV per dec, respectively. It seems that Pt/LSG_{200} showed inferior activity towards the HER over commercial Pt/C; however, the point to be noted here is based on the self-standing nature of the Pt/LSG_{200} electrodes. Furthermore, it can be improved by doping LSG electrodes by hetero-atoms and engineering the architecture of LSG to achieve the HER activity matching that of commercial Pt/C, which deserves future investigation.

The better performance of our Pt/LSG electrode toward the HER may be attributed to the strong chemical/electronic coupling between ALD Pt and LSG sheets. In addition, the growth of highly dispersed Pt nanoparticles on the 3D network of LSG yields numerous available active catalytic sites for the HER. The electronic coupling of highly dispersed ALD Pt with the underlying 3D network of LSG sheets with sufficient conductivity facilitates rapid electron transport. It was observed that the onset over-potential for the HER remained more or less the same (*i.e.*, between −0.03 and −0.05 V *vs.* the RHE) for the Pt/LSG electrodes prepared using different numbers of ALD cycles. However, at high HER current density (10 mA cm^{-2}), the over-potentials vary with the number of ALD Pt cycles. In contrast, the onset potential dramatically decreases to a lower value after 20 Pt ALD cycles liberating more cathodic current (Fig. 3d, Table S2†). With increased ALD cycles, the cathodic current density of the Pt/LSG_{200} electrode rose rapidly and approached that of commercial Pt/C.

The stability of the prepared Pt/LSG catalyst electrodes were further evaluated in acidic electrolyte. The electrodes were allowed to undergo LSV cycles continuously between −0.6 and 0.15 V in 0.5 M H_2SO_4 10 000 times, and finally the initial and final LSVs were compared, as shown in Fig. 4a. Note that the HER overpotential of Pt/LSG electrodes after 10 000 sweeps was almost the same as the initial overpotential. Also, a similar J–V curve along with very negligible loss of cathodic current is observed after the cycling test, thus demonstrating a very good stability of the Pt/LSG electrodes. In addition, the long-term stability of the Pt/LSG electrode was studied by extended

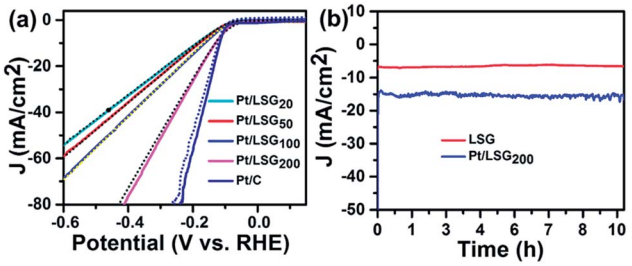

Fig. 4 (a) Comparison of LSV curves before and after stability measurements in 0.5 M H_2SO_4 (the dashed lines indicate the LSV recorded after 10 000 cycles, which is compared to the 1st LSV cycle (corresponding solid line)), (b) amperometric i–t plot of LSG and Pt/LSG_{200} at a constant potential of −0.6 and −0.2 V respectively showing high stability of current density over a period of 10 h.

electrolysis at fixed potentials in 0.5 M H_2SO_4 for a long time of 10 h (Fig. 4b). As an example, the stability of the Pt/LSG_{200} electrode was tested because of its high HER activity and compared with bare LSG electrodes. The catalytic current almost remained at −15 mA cm^{-2} at −0.2 V (*vs.* the RHE) for Pt/LSG_{200} and −0.7 mA cm^{-2} at −0.6 V for bare LSG electrodes, which reveals its excellent stability. It is worth mentioning that the hydrogen bubble formation on the Pt/LSG_{200} electrode was vigorous (see ESI, Video clip†), which resulted in noisy i–t data for Pt/LSG compared to bare LSG electrodes. Thus, the prepared Pt/LSG electrode materials displayed not only very high HER activity but also showed excellent stability in acidic electrolyte medium. Since device reproducibility is a decisive factor, we tested five different electrodes prepared using different ALD cycles. A negligible variance in the onset potential is observed, indicating very good reproducibility (shown in Fig. S5†). The high HER activity, good stability and reproducibility of the Pt/LSG electrodes can be attributed to the combination of following factors: (i) the good electrical conductivity of binder-free self-standing LSG electrodes, which allows for effective charge transfer (ii) the high electrochemically active surface area of LSG, which facilitates the ion adsorption and transport, and (iii) the synergistic effect between ALD Pt and 3D porous LSG, which plays an important role in the enhancement of HER activity with minimal Pt usage, and finally (iv) highly reproducible laser scribing and ALD processes.

Conclusion

In summary, a direct laser scribing strategy was developed to fabricate a self-standing, 3D network of graphene-like electrodes with conformal surface-coated Pt *via* atomic layer deposition for HER applications. These electrodes were found to be highly active for the hydrogen evolution reaction in acidic medium. The synergistic effect between ALD Pt and 3D porous LSG plays an important role in the enhancement of HER activity with minimal Pt usage, which is about one order of magnitude lower loading compared to the commercial Pt/C catalyst. In particular, the Pt/LSG_{200} electrode exhibits the lowest over-potential (−131 mV) reported at a current density of −10 mA

cm^{-2} in acidic media, which is very close to the benchmark Pt/C electrode (−118 mV, 10 wt% Pt catalyst). In addition, these electrodes exhibited long-term stability and good reproducibility in acidic media. Our 3D self-supporting electrode strategy, combined with ALD, opens a new pathway for scalable production of efficient water-splitting electrodes.

Experimental section

Reagents and materials

Porous LSG electrodes were fabricated by laser scribing over a commercial PI substrate (125 μm thickness). Trimethyl (methylcyclopentadienyl) platinum(IV) ($MeCpPtMe_3$) used as the Pt precursor and sulphuric acid (H_2SO_4) were purchased from Sigma Aldrich. A SYLGARD 184 silicone elastomer enclosing of a base elastomer/curing agent (Dow Corning) was mixed in a 10 (base) : 1 (curing agent) ratio by weight manually and was degassed by keeping under vacuum for 30 min in order to remove air bubbles prior to use as a passivation layer on LSG electrodes. Conducting silver paint was procured from TED Pella, USA. The reagents used in this study were of analytical grade and were used as received. All stock solutions were prepared using deionized water (18.2 MΩ cm, Milli-Q Direct, Merck Millipore, and Billerica, MA) without further purification.

Formation of laser scribed graphene scaffolds

Laser scribing was performed using a CO_2 Universal laser system (Universal X-660 laser cutter platform, λ = 1060 nm, pulse duration ~14 μs). The platform is equipped with a translational *X–Y* control stage with varying scan rates from 0.7 to 23 inches per s. The power can be varied from 2.4 to 5.4 W with the pulses per inch (PPI) in the range of 1 to 1000. Laser PPI can be controlled by the laser settings (100% corresponds to an absolute value of 1000 pulses per inch). For the fabrication of LSG electrodes, the laser settings including the peak power, speed, PPI and the *z*-distance between the laser source and the sample were optimized to be 15%, 10% and 1000 and 2 mm, respectively. Computer controlled Corel draw software was employed to design the LSG electrode patterns on a PI sheet. The laser beam size is roughly around 100 μm. Prior to use, the PI sheet was cleaned by rinsing with ethanol followed by water and then dried off by blowing nitrogen gas. All the electrode patterns were prepared under ambient conditions. Under these experimental conditions, the average thickness of the 3D porous LSG was found to be ~50 μm.

Atomic layer deposition of Pt

ALD of platinum on LSG electrodes was carried out using an Oxford Instruments ALD system (FlexAL), which provides both thermal and remote plasma enhanced ALD configurations. Commercially available trimethyl(methylcyclopentadienyl) platinum(IV) ($Pt(MeCp)Me_3$, Sigma-Aldrich Ltd.) was used as the platinum precursor and inductively coupled plasma (ICP) of oxygen was used as the reactant. The temperature of the precursor was maintained at 70 °C. $Pt(MeCp)Me_3$ vapor was carried into the process chamber through Ar bubbler gas at a flow rate of 150 sccm. The ALD process of platinum follows the standard deposition cycle sequence: first a pulse of Pt precursor vapor is introduced, followed by an Ar gas purge, and then a pulse of oxygen plasma, followed by another Ar gas purge. A modification to the above mentioned standard ALD process was made by inserting a $Pt(MeCp)Me_3$ precursor soaking step between the platinum precursor pulse step and the following Ar gas purge step to prolong the dwell time of the precursor. This soaking step reduces the platinum precursor usage and helps to achieve a self-limited Pt growth on the LSG electrode surface. The deposition temperature was maintained at 200 °C. The following ALD process parameters were used: a precursor pulse time of 0.7 s, a soaking step of 3 s after the platinum precursor valve is closed, an oxygen plasma step of 3 s, and both ALD chamber purge steps after platinum dose and oxygen plasma of 3 s. Different platinum-loaded LSG substrates were prepared by varying the deposition cycles from 20 to 200. These prepared electrodes are henceforth referred to as Pt/LSG_{20}, Pt/LSG_{50}, Pt/LSG_{100}, and Pt/LSG_{200} in the manuscript.

Material characterization

X-ray diffraction (XRD) patterns were measured using a Bruker diffractometer (D8 Advance) with Cu Kα radiation, $\lambda = 1.5406$ Å. The morphology and microstructure of the Pt/LSG based electrodes were characterized by high-resolution field emission scanning electron microscopy (FESEM) (Nova Nano 630, FEI). An energy-dispersive X-ray spectroscopy (EDX) column equipped with the SEM was used to do elemental analysis and also mapping to see the uniform coverage of Pt. Cross-sectional SEM was employed to measure the thickness of LSG and Pt/LSG films. Raman spectroscopy measurements were carried out on the samples using a micro-Raman spectrometer (LabRAM ARAMIS, Horiba-Jobin Yvon). Raman spectra were acquired with notch filters cutting at 100 cm^{-1} using a Cobalt laser (473 nm, 5 mW at the source) with a laser spot size of 1.5 μm. Raman mapping was done by continuous acquiring of spectra in a given scanning area (in this case 10 × 10 μm^2) with an adjacent spacing of 2 μm. Furthermore, the acquired Raman data was processed to generate I_D/I_G map in order to know the defect distribution over a selected region of Pt/LSG.

Electrochemical characterization

The electrochemical HER activity of LSG based electrodes was evaluated using a three-electrode electrochemical cell comprising a Pt wire counter electrode, Ag/AgCl (3 M KCl) as the reference electrode and LSG or Pt/LSG as the working electrode using a CHI 6008 D electrochemical workstation (Austin, USA) at a scan rate of 5 mV s^{-1}. The physical area of the working electrode was defined (3 mm dia) using a thin-layer of polydimethylsiloxane (PDMS) which prevents contact of the electrolyte with the rest of the electrode area, as shown in the ESI, Fig. S1a.† All the tests were performed in 0.5 M H_2SO_4 electrolyte in the potential range from 0 to −0.6 V. For the stability study, the initial voltammogram was recorded at a scan rate of 5 mV s^{-1} followed by 10 000 cycles at a scan rate of 100 mV s^{-1}, followed by linear sweep voltammetry (LSV) at a 5 mV s^{-1} scan

rate. Amperometric *i–t* measurement was carried out on LSG and Pt/LSG in order to study the stability of the current over time. All measurements were conducted under ambient conditions. The potential *vs.* Ag/AgCl was converted to the reversible hydrogen electrode (RHE) using the Nernst equation: $E_{RHE} = E_{Ag/AgCl} + 0.059\ pH + E^{o}_{Ag/AgCl}$, for 0.5 M H_2SO_4, $E_{RHE} = E_{Ag/AgCl} + 0.21$ V.

Conflicts of interest

There are no conflicts to declare.

Acknowledgements

Research reported in this publication is supported by funding from the King Abdullah University of Science and Technology (KAUST), Saudi Arabia. Dr P. Nayak would like to thank the DST (Government of India) for the Inspire Faculty Award (Grant No. 04/2015/002660).

Notes and references

1 M. S. Dresselhaus and I. L. Thomas, *Nature*, 2001, **414**, 332.
2 J. A. Turner, *Science*, 1999, **285**, 687.
3 J. A. Turner, *Science*, 2004, **305**, 972.
4 Y. Jiao, Y. Zheng, M. Jaroniec and S. Z. Qiao, *Chem. Soc. Rev.*, 2015, **44**, 2060.
5 S. Chu and A. Majumdar, *Nature*, 2012, **488**, 294.
6 N. Armaroli and V. Balzani, *Angew. Chem., Int. Ed.*, 2007, **46**, 52.
7 T. Abbasi and S. A. Abbasi, *Renewable Sustainable Energy Rev.*, 2011, **15**, 3034.
8 M. Li, Q. Ma, W. Zi, X. Liu, X. Zhu and S. Liu, *Sci. Adv.*, 2015, **1**, 1400268.
9 W. Sheng, Z. Zhuang, M. Gao, J. Zheng, J. G. Chen and Y. Yan, *Nat. Commun.*, 2015, **6**, 5848.
10 J. Zheng, W. Sheng, Z. Zhuang, B. Xu and Y. Yan, *Sci. Adv.*, 2016, **2**, 1501602.
11 S. E. Moradi, *Chem. Biochem. Eng. Q.*, 2016, **30**, 1.
12 D. Jasion, J. M. Barforoush, Q. Qiao, Y. Zhu, S. Ren and K. C. Leonard, *ACS Catal.*, 2015, **5**, 6653.
13 T. Brulle, A. Denisenko, H. Sternschulte and U. Stimming, *Phys. Chem. Chem. Phys.*, 2011, **13**, 12883.
14 Y. Ito, W. Cong, T. Fujita, Z. Tang and M. Chen, *Angew. Chem., Int. Ed. Engl.*, 2015, **54**, 2131.
15 Y. Y. Chen, Y. Zhang, W. J. Jiang, X. Zhang, Z. Dai, L. J. Wan and J. S. Hu, *ACS Nano*, 2016, **10**, 8851.
16 Y. Zheng, Y. Jiao, L. H. Li, T. Xing, Y. Chen, M. Jaroniec and S. Z. Qiao, *ACS Nano*, 2016, **10**, 5290.
17 D. H. Youn, S. Han, J. Y. Kim, J. Y. Kim, H. Park, S. H. Choi and J. S. Lee, *ACS Nano*, 2014, **8**, 5164.
18 H. Dong, C. Liu, H. Ye, L. Hu, B. Fugetsu, W. Dai, Y. Cao, X. Qi, H. Lu and X. Zhang, *Sci. Rep.*, 2015, **5**, 17542.
19 Y. Jia, L. Zhang, A. Du, G. Gao, J. Chen, X. Yan, C. L. Brown and X. Yao, *Adv. Mater.*, 2016, **28**, 9532.
20 S. Mao, G. Lu and J. Chen, *Nanoscale*, 2015, **7**, 6924.
21 P. Nayak, B. Anbarasan and S. Ramaprabhu, *J. Phys. Chem. C*, 2013, **117**, 13202.
22 Y. Wang, Y. Wu, Y. Huang, F. Zhang, X. Yang, Y. Ma and Y. Chen, *J. Phys. Chem. C*, 2011, **115**, 23192.
23 N. P. Dasgupta, C. Liu, S. Andrews, F. B. Prinz and P. Yang, *J. Am. Chem. Soc.*, 2013, **135**, 12932.
24 S. Saha, B. Martin, B. Leonard and D. Li, *J. Mater. Chem. A*, 2016, **4**, 9253.
25 K. P. Katuri, N. M. Bettahalli, X. Wang, G. Matar, S. Chisca, S. P. Nunes and P. E. Saikaly, *Adv. Mater.*, 2016, **28**, 9504.
26 J. Lin, Z. Peng, Y. Liu, F. Ruiz-Zepeda, R. Ye, E. L. Samuel, M. J. Yacaman, B. I. Yakobson and J. M. Tour, *Nat. Commun.*, 2014, **5**, 5714.
27 P. Nayak, N. Kurra, C. Xia and H. N. Alshareef, *Adv. Electron. Mater.*, 2016, **2**, 1600185.
28 C. E. Banks, T. J. Davies, G. G. Wildgoose and R. G. Compton, *Chem. Commun.*, 2005, **7**, 829.
29 P. Nayak and S. Ramaprabhu, *J. Phys. Chem. C*, 2015, **119**, 2917.
30 M. Baro, P. Nayak, T. T. Baby and S. Ramaprabhu, *J. Mater. Chem. A*, 2013, **1**, 482.
31 A. C. Ferrari and J. Robertson, *Phys. Rev. B*, 2000, **61**, 14095.
32 N. Kurra, A. A. Sagade and G. U. Kulkarni, *Adv. Funct. Mater.*, 2011, **21**, 3836.
33 N. Kurra and G. U. Kulkarni, *Lab Chip*, 2013, **13**, 2866.
34 M. A. Pimenta, G. Dresselhaus, M. S. Dresselhaus, L. G. Cancado, A. Jorio and R. Saito, *Phys. Chem. Chem. Phys.*, 2007, **9**, 1276.